Int. J. Electrochem. Sci., 7 **(2012)** 10592 - 10606

International Journal of
ELECTROCHEMICAL
SCIENCE
www.electrochemsci.org

Durability of Ordered Mesoporous Carbon Supported Pt Particles as Catalysts for Direct Formic Acid Fuel Cells

Chuntao Liu[1], *Meng Chen*[2], *Chunyu Du*[3,*], *Jing Zhang*[2], *Geping Yin*[3], *Pengfei Shi*[3], *Yongrong Sun*[1]

[1] School of Chemistry and Materials Science, Heilongjiang University, 150080 Harbin, China
[2] College of Materials Science and Chemical Engineering, Harbin Engineering University, 150001 Harbin, China
[3] School of Chemical Engineering and Technology, Harbin Institute of Technology, 150001 Harbin, China
[*]E-mail: cydu@hit.edu.cn

Received: 31 August 2012 / *Accepted:* 29 September 2012 / *Published:* 1 November 2012

This paper examines the possibility of ordered mesoporous carbon (OMC) supported Pt particles (Pt/OMC) as catalysts for direct formic acid fuel cells (DFAFCs), with focus on the durability issue. The Pt/OMC catalyst was synthesized by a microwave-assisted polyol approach, and characterized by transmission electron microscopy, X-ray diffraction and X-ray photoelectron spectroscopy. It is shown that the high surface area and mesopores of OMC support lead to smaller average size and better dispersion of Pt nanoparticles. In addition, OMC support facilitates the deposition of more metallic Pt particles. The ageing test of cyclic voltammetry (CV) reveals that Pt/OMC exhibits higher long-term durability than Pt/C, due to the confining effects of mesopores in OMC on Pt particles. Further, linear sweeping voltammetry measurements show that the Pt/OMC catalyst has highly stable and robust activity for oxygen reduction reaction, which is suggested to be related to the tailoring by OMC support. In contrast, it is demonstrated that the Pt/OMC catalyst is less durable towards the reaction of formic acid oxidation. Therefore, the Pt/OMC catalyst is promising as durable and robust cathode catalyst for DFAFCs.

Keywords: ordered mesoporous carbon, fuel cell, oxygen reduction, formic acid oxidation, durability.

1. INTRODUCTION

Direct liquid-feed fuel cells have been viewed as a promising technology for portable power sources because liquid fuels are easy to store, transport and refill, and allow for compact design that can offer quite high energy density [1]. Among various direct liquid-feed fuel cells, the direct formic acid fuel cell (DFAFC) has recently attracted much interest because formic acid has many merits over

other liquid fuels such as methanol [2-4]: (1) formic acid is safer and easier to handle; (2) electrooxidation of formic acid is more efficient; (3) formic acid suffers less crossover through the membrane, so that the optimal operating concentration can be high, leading to improved power density. Thus, the DFAFC will hopefully become one of the earliest commercialized small fuel cells.

Unfortunately, before becoming commercially viable, the DFAFC still faces several technical challenges. Among them, the most critical one is more active and durable catalysts for the reactions of formic acid oxidation (FAO) and oxygen reduction (OR). Nowadays, Pt nanoparticles supported on carbon black (Pt/C) are usually used as the DFAFC catalysts. On the one hand, the sluggish kinetics of FAO and OR reactions on the Pt/C catalyst has to be further improved; on the other hand, the severe performance degradation of Pt/C catalyst during fuel cell operation needs remarkable alleviation [5-7]. Using alternative catalyst supports to replace carbon black has been proved to be effective in improving the activity and durability of their supported catalysts [8,9].

Ordered mesoporous carbons (OMCs) have recently shown great potentials in a wide range of applications, due to their ordered pore structures, high surface areas, large pore volumes, high electrical conductivity and good chemical stability [10,11]. Some pioneering works have revealed that OMCs are intriguing as catalyst support materials in fuel cell electrodes [12,13]. Ryoo et al. [14] first reported the usage of OMCs as catalyst supports, and demonstrated that Pt nanoparticles supported on CMK-5 type OMC exhibited superior catalytic activity towards OR reaction compared with those dispersed on conventional carbon black. Subsequently, several studies confirmed that noble metal nanoparticles supported on OMCs had promising catalytic activities for both OR and methanol oxidation reactions [15-18]. However, it is noteworthy that although previous studies demonstrated the promise of OMCs as new forms of catalyst supports, they concentrated mainly on hydrogen or direct methanol fuel cells and no usage of OMC for the DFAFC was reported. More importantly, the durability issue of OMC supported catalysts is still not paid much attention, which is crucial to the extended period of fuel cell operating.

The aim of this study is to explore the possibility of OMC supported Pt nanoparticles (Pt/OMC) as the OR and FAO catalysts for the DFAFC, with focus on their durability. Firstly, CMK-3 type OMC was synthesized by a hard template method. Then, the Pt/OMC catalyst with 20% Pt loading was prepared by a microwave-assisted polyol reduction approach. Afterwards, the CMK-3 type OMC support and the Pt/OMC catalyst were characterized by transmission electron microscopy (TEM), X-ray diffraction (XRD) and X-ray photoelectron spectroscopy (XPS). The durability of the Pt/OMC catalyst towards OR and FAO reactions was finally evaluated and analyzed by comparing its electrochemical behaviors with those of the Pt/C catalyst. It was indicated that the Pt/OMC catalyst was promising as a long-term durable and robust catalyst for the cathode of DFAFCs.

2. EXPERIMENTAL

2.1. Synthesis

Mesoporous silica SBA-15, used as the hard template for the synthesis of CMK-3 type OMC, was synthesized according to the procedure reported in the literature [19]. In brief, 4.0 g of Pluronic

123 triblock co-polymer (Aldrich) was dissolved in 30 ml of deionized water by stirring at room temperature for 1 h. Then, 120 ml of 2 M HCl solution and 8.5 g of tetraethylorthosilicate (Aldrich) were added to the solution with stirring at 40 ^{o}C for 20 h. After the mixture was aged at 100 ^{o}C for 24 h, the white powder was obtained through filtration, washing and drying under vacuum. The product was finally calcined at 550 ^{o}C for 5 h under air to remove the organic template to obtain the SBA-15 template. The CMK-3 type OMC was replicated from the SBA-15 template with sucrose as carbon source. Specifically, 0.95 g of sucrose, 0.06 g of H_2SO_4 and 4.0 g of H_2O were impregnated into 0.76 g of SBA-15 by an incipient wetness method under vacuum. Afterwards, the mixture was dried at 100 ^{o}C for 6 h and subsequently 160 ^{o}C for 6 h. The impregnation-drying procedure was repeated twice to completely infiltrate the internal pores of SBA-15 template with the carbon source. The mixture was then heated to 900 ^{o}C and carbonized for 2 h under Ar gas. Finally, the SBA-15 template was dissolved by 50 ml of 10% HF, and the CMK-3 OMC was obtained by filtering, washing with ethanol, and drying at 100 ^{o}C for 3 h.

The Pt/OMC catalyst was prepared by a microwave assisted polyol method [20]. Briefly, 39 mg of CMK-3 OMC support was firstly mixed with 40 ml of ethylene glycol and 10 ml of isopropanol to form a homogeneous ink by ultrasonic agitating for 7 h. Then, 0.5 ml of 0.1 M H_2PtCl_6 solution was added into the ink and the mixture was kept in stirring state for 3 h. After that, pH value of the mixture was adjusted to 11 by 2 M NaOH solution, and the mixture was subsequently subject to microwave-heating (2450 MHz, 800 W) for 1 min. After cooling down to room temperature, pH value of the mixture was adjusted to 3.5 by 1 M HNO_3 solution. Finally, the catalyst was filtered, washed and dried under vacuum for 12 h. For the sake of comparison, conventional Pt/C catalyst was also prepared by the same procedure except that CMK-3 type OMC was replaced by Vulcan XC-72 carbon black (Cabot).

2.2. Characterization and measurements

XRD patterns of the samples were collected on a Rigaku D/MAX-3B X-ray diffractometer with Cu Kα radiation. The mesostructure of the CMK-3 OMC was characterized using the small-angle X-ray scattering (SAXS) technique on a Bruker D8 Advance X-ray diffractometer. TEM characterization was performed using a transmission electron microscope (Hitachi model H-800 system) operated at 200 kV. The Pt loading in the electrocatalysts was obtained by energy dispersive X-ray analyses (EDX) technique coupled to a JEM 100CX-II scanning electron microscope. The surface chemical composition of the samples was determined by XPS on a VG ESCALAB 250 spectrometer (Thermo Electron) using a non-monochromatized Al Kα X-ray source.

Electrochemical tests were performed on a rotating disk electrode (RDE) apparatus (Princeton Applied Research) in a three-compartment electrochemical cell with a Pt foil and an Hg/Hg_2SO_4 electrode serving as the counter and reference electrodes, respectively. Prior to each experiment, a suspension of the samples was prepared as follows: To 3.5 mg of dried samples (e.g., Pt/OMC), 2.7 mL of deionized water, 0.725 ml of isopropanol and 0.075 ml of 5% (w/w) Nafion solution in alcohol were added; The resulting mixture was sonicated for 30 min. 12.5 μl of the sample suspension was

coated onto a 4 mm diameter glassy carbon RDE, and the RDE was then dried at 50 ^{o}C under a nitrogen atmosphere for 30 min.

Before electrochemical tests, a pretreatment of the sample-coated electrodes was preformed to activate the electrodes by cycling them between 0.05 and 1.2 V for 50 cycles at a scan rate of 50 mV s^{-1} in N_2-purged 0.1 M $HClO_4$ solution. To assess the catalyst durability, cyclic voltammetry (CV) was carried out between 0.6 and 1.2 V at a scan rate of 50 mV s^{-1} in N_2-purged 0.1 M $HClO_4$ solution. The electrochemically active surface area (EASA) of the catalysts was evaluated by the H-desorption peaks in the profiles of CV conducted at a scan rate of 50 mV s^{-1} between 0.05 and 1.2 V in N_2-saturated 0.1 M $HClO_4$ solution. The OR activity was measured by linear sweeping voltammetry (LSV) in O_2-saturated 0.1 M $HClO_4$ solution or 0.1 M $HClO_4$ + 10 μM HCOOH solution at a scan rate of 5 mV s^{-1} from open circuit voltage to 0 V. The FAO activity was measured by CV in N_2-purged solution of 0.1 M $HClO_4$ and 0.5 M formic acid at a scan rate of 50 mV s^{-1} between 0.05 and 1.1 V. The steady-state anodic polarization curves of the OMC and Vulcan XC-72 supports were obtained in N_2-purged 0.1 M $HClO_4$ solution by stepping the electrode to the desired potentials and stabilizing for up to 15 min at each potential. All the electrochemical measurements were performed at room temperature, and the potentials were quoted with respect to the reversible hydrogen electrode (RHE).

3. RESULTS AND DISCUSSION

Fig. 1 shows TEM image and XRD pattern of the CMK-3 type OMC support. From the TEM image (Fig. 1A), it was confirmed that the OMC support possessed delicate and parallel arrays of uniform mesopores with pore size of ~8 nm. From the XRD pattern (Fig. 1B), two broad diffraction peaks corresponding to the (002) and (101) diffractions of graphitic carbon could be seen at ~22.5º and ~43.7º, respectively, which was similar to the pattern of SBA-15 [21].

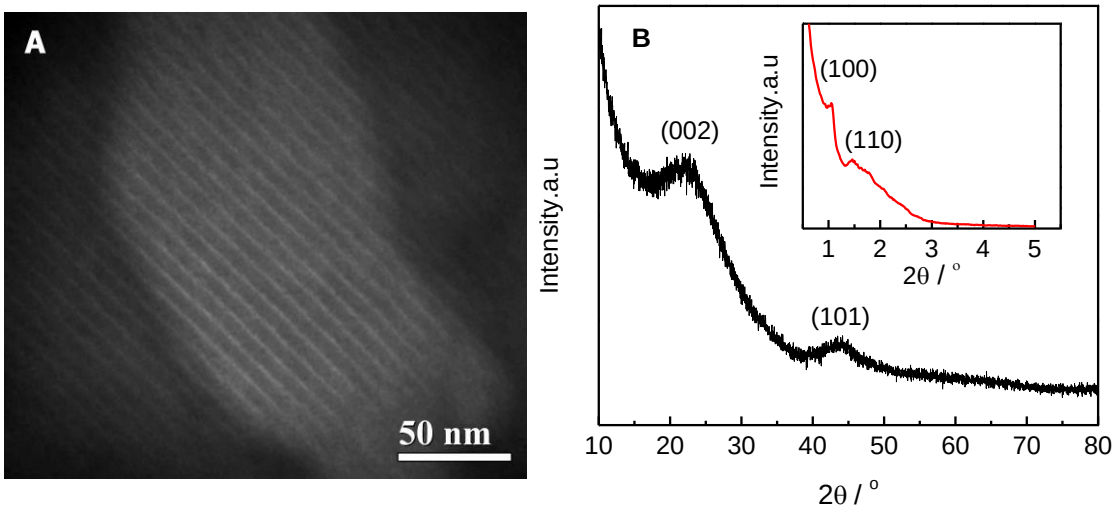

Figure 1. TEM image (A) and XRD pattern (B) of the OMC support. Inset: SAXS pattern of the OMC support

Further, no peaks corresponding to the (004) and (110) diffractions could be observed at ~53º and ~78º, suggesting that the OMC had a turbostratic structure with a large curvature of the graphene layers [22]. The SAXS pattern of the OMC support shown in inset of Fig. 1B displayed well-resolved (100) and (110) peaks and demonstrated the presence of ordered hexagonal pore arrays with mesoporous structure [23], which was consistent with the TEM observation.

Fig. 2A and 2B show TEM images of the Pt/OMC and Pt/C catalysts with Pt loading of 19.2% and 19.5%, respectively. Pt nanoparticles were observed to be uniformly dispersed on the two supports. The sizes of Pt particles were estimated from measurements of randomly taken 200 particles and the corresponding histograms are shown in Fig. 2C and 2D. It was revealed that the particle size distribution was narrow with majority of Pt particles around 2-3 nm for both the two catalysts. The average size of Pt particles was estimated to be 2.48 and 2.75 nm on OMC and Vulcan XC-72 supports, respectively, indicating that the Pt particles on OMC support was slightly smaller than those on Vulcan XC-72. The specific surface area of Pt nanoparticles could be roughly calculated according to the following equation [24]:

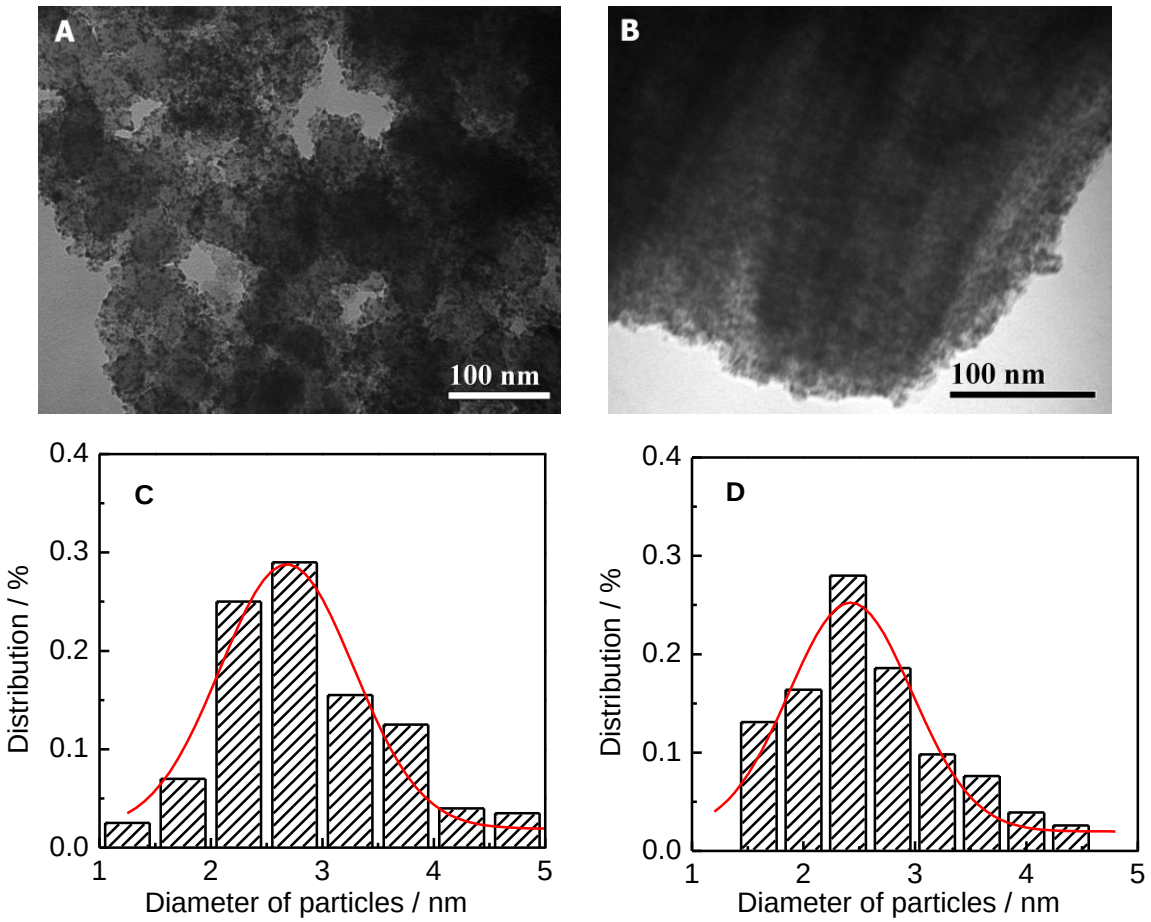

Figure 2. TEM images of Pt/C (A) and Pt/OMC (B), and histograms of Pt particles for Pt/C (C) and Pt/OMC (D)

$$S = \frac{6000}{\rho d} \qquad (1)$$

where S (m^2 g^{-1}) is the specific surface area of Pt particles, ρ (21.4 g cm^{-3}) is the Pt density and d (nm) is the average particle size. Thus obtained values were 101.8 and 115.6 m^2 g^{-1} for Pt/C and Pt/OMC catalysts, respectively, indicating that Pt particles were slightly better dispersed on OMC than on Vulcan XC-72. This result demonstrated that the high surface area along with the ordered pores of OMC support could accommodate a large amount of Pt particles, thus leading to a high dispersion of Pt particles [25].

Fig. 3 gives XRD patterns of the Pt/OMC and Pt/C catalysts. The patterns exhibited diffraction peaks at 2θ values of around 39.8º, 46.3º, 67.5º, and 81.3º, which corresponded to (111), (200), (220) and (311) facets of the face centered cubic Pt, respectively, suggesting that Pt was mainly present in the metallic state on both OMC and Vulcan XC-72 supports. The average size of Pt nanocrystallites was estimated using Scherrer equation [24]:

$$d = \frac{0.9\lambda}{\beta \cos(\theta)} \qquad (2)$$

where λ is the X-ray wavelength, β is the half-peak width for the (220) peak in radians, and θ is the Bragg angle of the (220) peak. Thus calculated values were 2.42 and 2.65 nm for Pt/OMC and Pt/C, respectively, which were roughly consistent with the TEM results.

XPS survey spectra of the Pt/OMC and Pt/C catalysts were recorded and the corresponding wide spectra (not shown herein) confirmed the presence of Pt, C and O elements. Fig. 4 depicts the detailed Pt4f spectra for the Pt/OMC and Pt/C catalysts, which could be deconvoluted into three pairs of peaks labeled with I, II, and III. Peaks I at binding energy of 71.1 (Pt4f7/2) and 74.4 eV (Pt4f5/2) were attributed to metallic Pt, peaks II at around 72.4 and 75.7 eV was assigned to Pt^{2+} chemical state in either PtO or $Pt(OH)_2$ form, while peaks III at around 74.2 and 77.7 eV were ascribed to Pt^{4+} species such as PtO_2 [26].

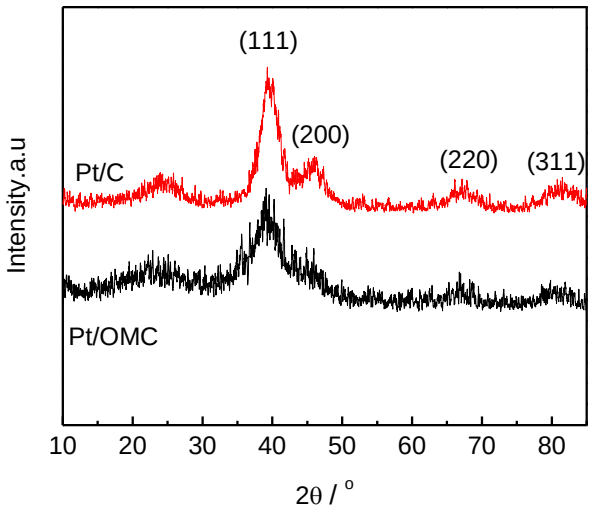

Figure 3. XRD patterns of the Pt/OMC and Pt/C catalysts

The integration of peak areas can give surface compositions of Pt particles and the results are shown in Table 1. It was clear that most Pt species on the surface of Pt particles exist as metallic Pt for the two catalysts. However, the metallic Pt content for Pt/OMC was 18% higher than that for Pt/C, suggesting that OMC support facilitated the deposition of metallic Pt. This difference indicated more facile electron transfer from the OMC support to Pt particles, which resulted from the unique surface chemistry of the OMC material.

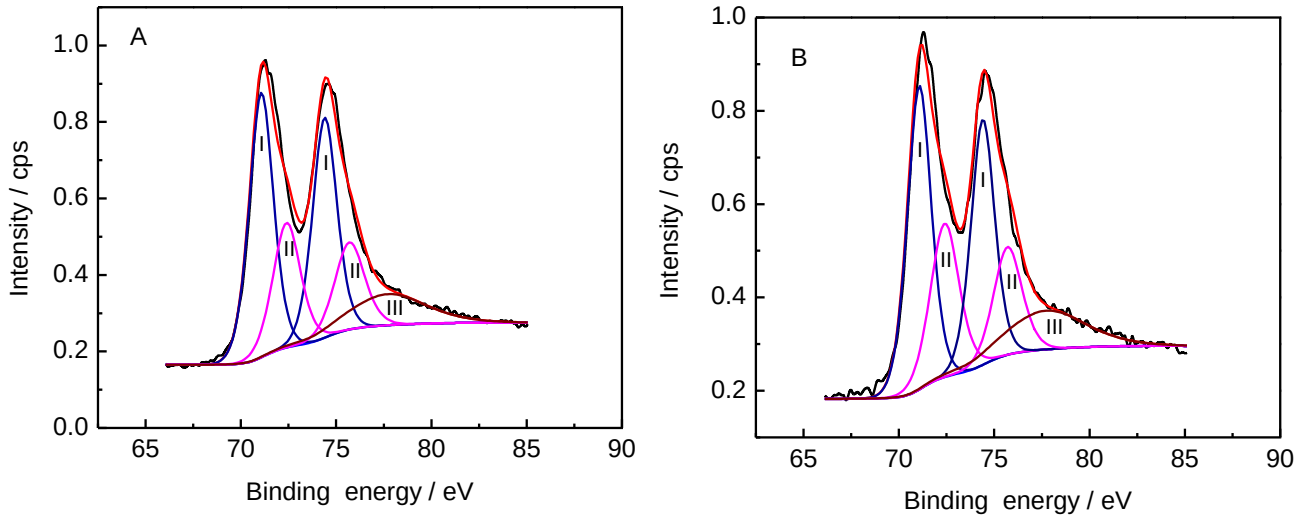

Figure 4. Pt 4f spectra for the Pt/OMC (A) and Pt/C (B) catalysts

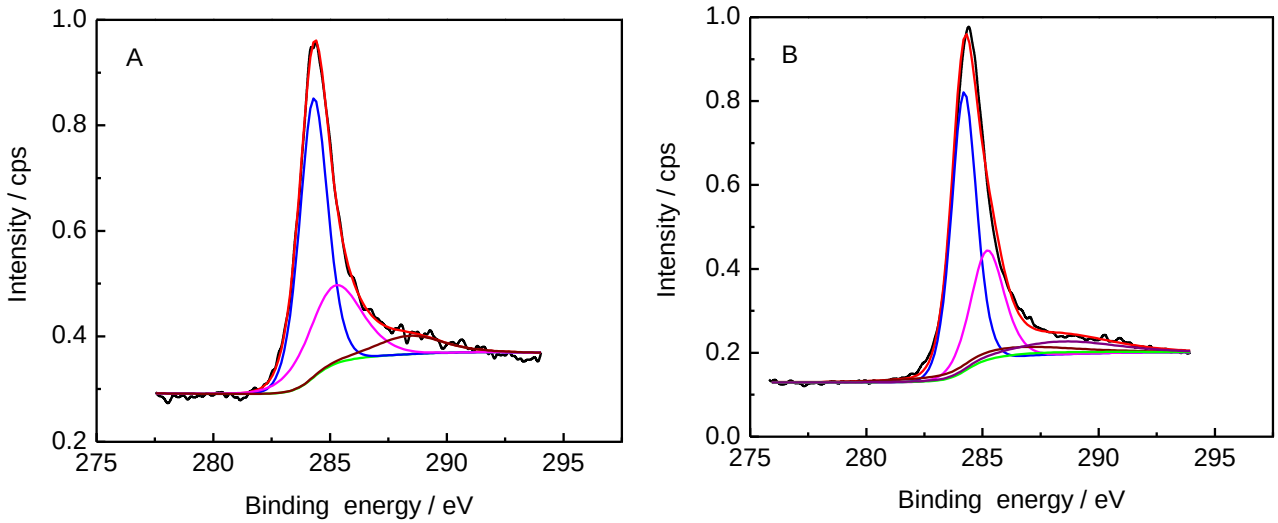

Figure 5. C1s spectra of the OMC (A) and Vulcan XC-72 (B) supports

Fig. 5 shows C1s spectra of the OMC and Vulcan XC-72 supports and their tentative deconvolution results. The binding energies for sp2 and sp3 hybridized carbon were assigned at 284.3 and 285.2 eV, while those for functional groups of C–OH, C=O and COOH were respectively assigned

at 286.10, 287.6 and 288.4 eV [27], although the actual values for these functional groups should have some distributions. The surface compositions of the two supports from the integration of deconvoluted peak areas are also presented in Table 1. From Table 1, it could be seen that the OMC support exhibited the existence of significantly less surface oxygenic functional groups. This was likely due to the fact that the functional groups on OMC surface were largely eliminated during the carbonization process, which would affect the catalyst durability because the functional groups are effective in the anchorage of Pt particles and thus enhance the stability of Pt particles supported [28].

Table 1. Surface compositions of CMK-3 type OMC and Vulcan XC-72 and their supported Pt nanoparticles

	Pt^0	Pt^{2+}	Pt^{4+}	C (sp^2)	C (sp^3)	-C-OH	-C=O	-COOH
OMC	58.12%	30.03%	11.85%	59.22%	31.06%	0	0	9.18 %
Vulcan XC-72	49.35%	37.51%	13.13%	51.89%	27.44%	8.85%	1.79%	10.02%

To evaluate the durability of Pt/OMC catalyst, the Pt/OMC and Pt/C catalysts were subject to various cycles of durability tests in 0.1 M $HClO_4$ solution between 0.6 and 1.2 V. Fig. 6A and 6B show CV curves of the two catalysts in 0.1 M $HClO_4$ solution after the durability tests. The cathodic and anodic peaks between 0.05 and 0.4 V were assigned to the adsorption and desorption of hydrogen, while the anodic plateau and cathodic peak above 0.4 V corresponded to the oxidation of Pt and the reduction of Pt oxide, respectively. The double layer capacity between 0.4 and 0.7V for the Pt/OMC catalyst was apparently higher than that for the Pt/C one, consistent with the larger surface area of the OMC support. Before durability tests, the two pristine catalysts exhibited similar profiles for H-adsorption/desorption, but slightly different profiles for Pt oxidation and Pt oxide reduction. This result indicated that the Pt particles supported on OMC and Vulcan XC-72 had different capabilities of electron gain and loss, which was due to the support tailoring as revealed by XPS results and would affect the activity and durability of Pt particles. After 1000 cycles of durability tests, H-adsorption/desorption behaviors on the two catalysts were significantly distinctive. The Pt/C catalyst still exhibited a large peak for strong H-desorption at 0.14 V and a small peak for weak H-desorption at 0.20 V, whereas the Pt/OMC one showed two comparable peaks for both strong and weak H-desorption. Kinoshita et al. reported that H-adsorption/desorption behaviors depended highly on the surface crystallinity of Pt catalyst [29]. Such a change in the shape of H-desorption peaks was obviously related to the development of different surface crystallinities tailored by the distinct support features during the durability tests.

EASA of the Pt/OMC and Pt/C catalysts during durability tests was calculated by integrating the charge corresponding to the H-desorption peak after the double-layer correction using the following equation [24]:

$$\text{EASA} = \frac{Q_{\text{H}}}{[\text{Pt}] \times 0.21} \qquad (3)$$

where Q_{H} is the integral charge for hydrogen desorption (mC cm^{-2}), [Pt] represents the platinum loading (mg cm^{-2}) in the electrode and 0.21 is the charge required to oxidize a monolayer of H on Pt surface (mC cm^{-2}). Thus obtained EASA values are shown in Fig. 6C and revealed a general trend of significant loss with extending the durability tests. Initially, the EASA of Pt/OMC was higher than that of Pt/C. During the first 500 cycles of durability tests, this value was decreased to be lower than that of Pt/C. After 500 cycles, however, the decrease rate for Pt/OMC was greatly alleviated, whereas that for Pt/C was still significant. This result indicated that the Pt/OMC catalyst was a durable catalyst for long-term running rather than for short-term running.

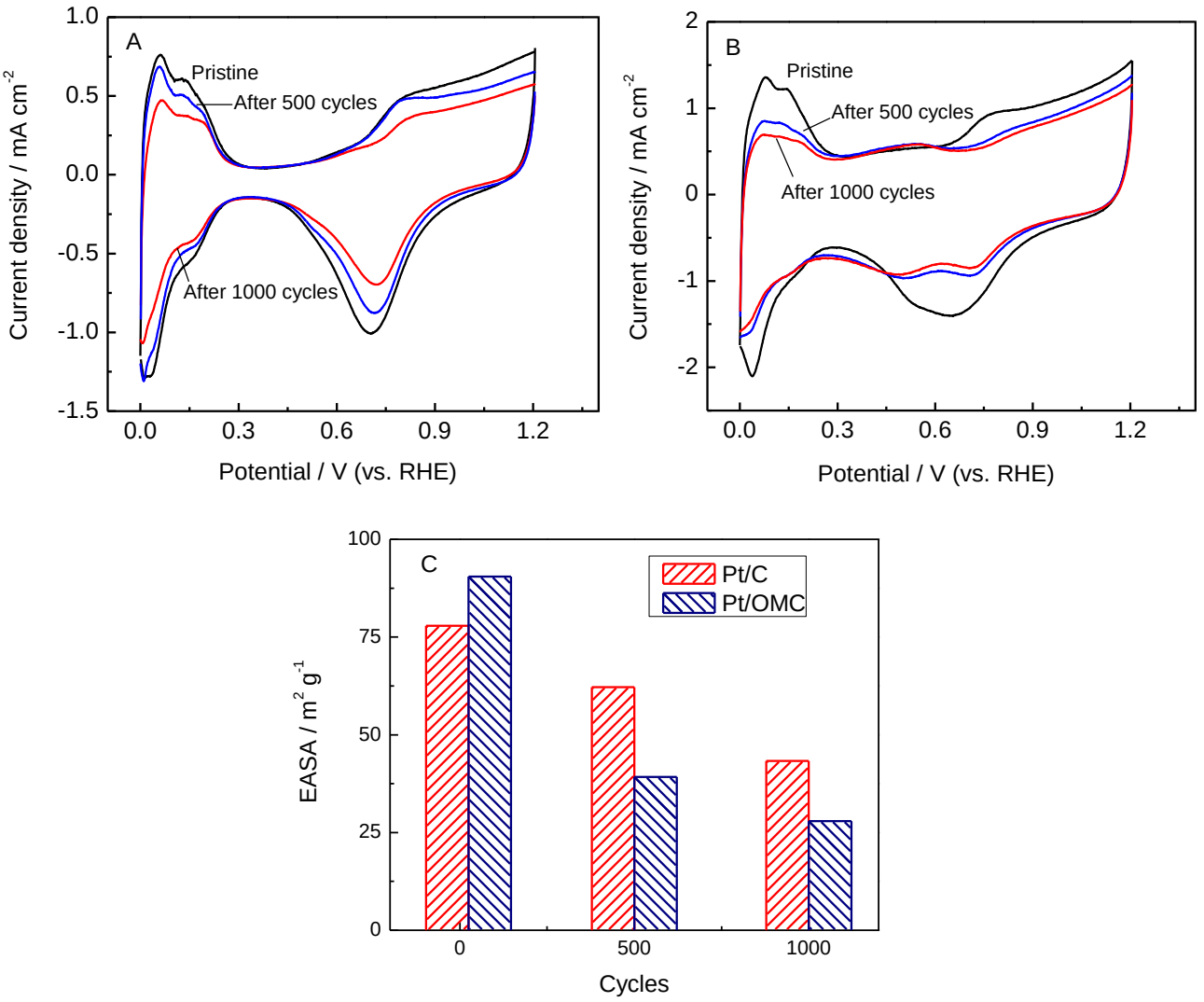

Figure 6. CV curves of Pt/C (A) and Pt/OMC (B) catalysts after different cycles of durability tests in 0.1 M $HClO_4$ solution at a scan rate of 50 mV s^{-1}, and EASA of the Pt/OMC and Pt/C catalysts vs. cycle number (C)

In order to detect the reasons for the EASA loss, the morphology of the Pt/OMC and Pt/C catalysts was characterized after 1000 cycles of durability tests, and the corresponding TEM images are presented in Fig. 7A and 7B. In comparison with the pristine catalysts in Fig. 2, the majority of small Pt particles disappeared and their size increased substantially after the durability tests. The histograms of Pt particles in the TEM images are shown in Fig. 7C and 7D, respectively. It was evident that the average particle size increased remarkably, and the distribution of Pt particle sizes became broader for the two catalysts. Further, it could be seen that the average particle size for Pt/OMC was a little larger than that for Pt/C, which was closely related to the appearance of more large Pt particles of >10 nm on the surface of Pt/OMC. This appearance was mainly due to the reduced functional groups on the OMC surface and the serious corrosion of the OMC support as demonstrated by the steady-state anodic currents shown in Fig. 8.

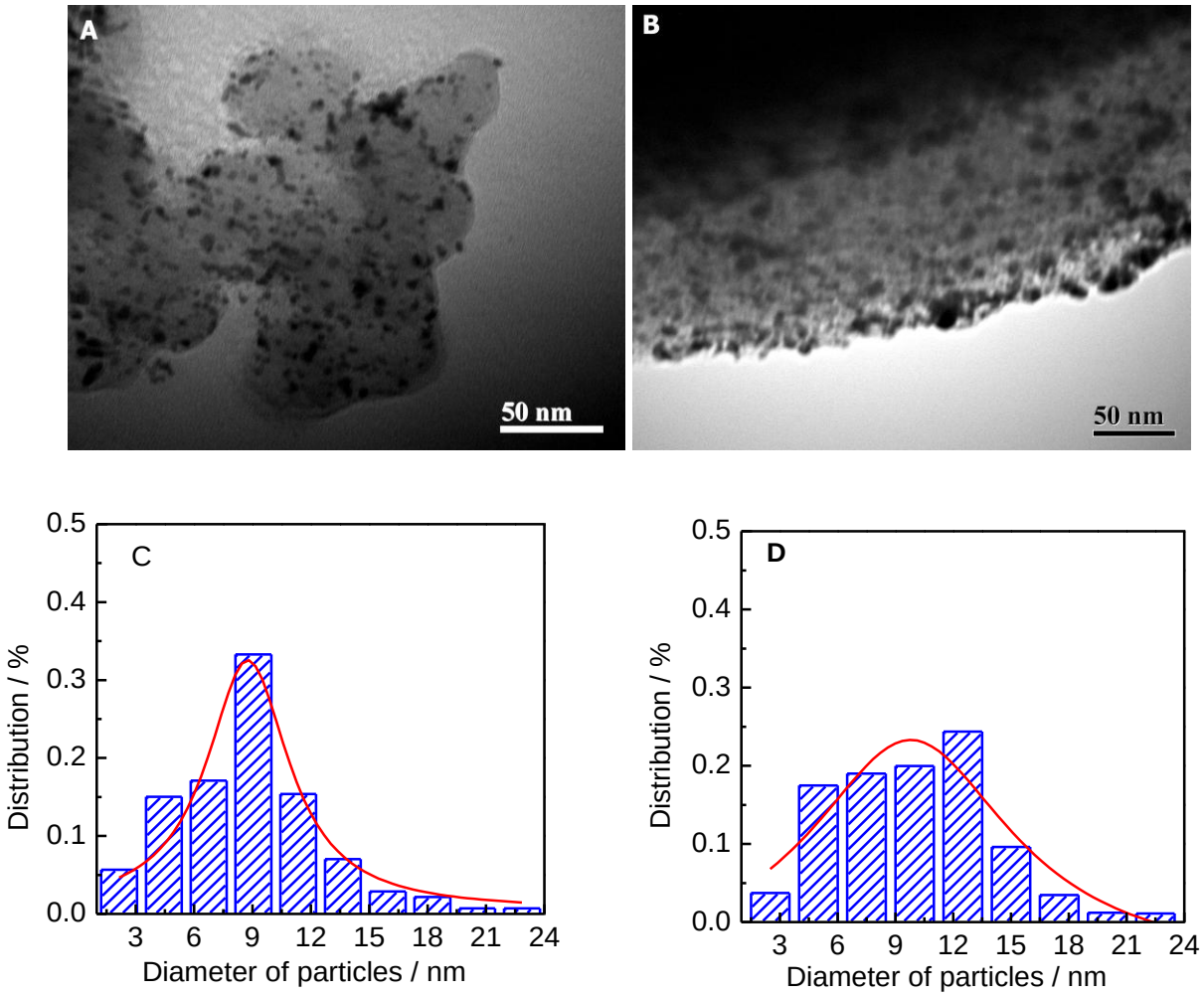

Figure 7. TEM images of Pt/C (A) and Pt/OMC (B), and histograms of Pt particles for Pt/C (C) and Pt/OMC (D), after 1000 cycles of durability tests

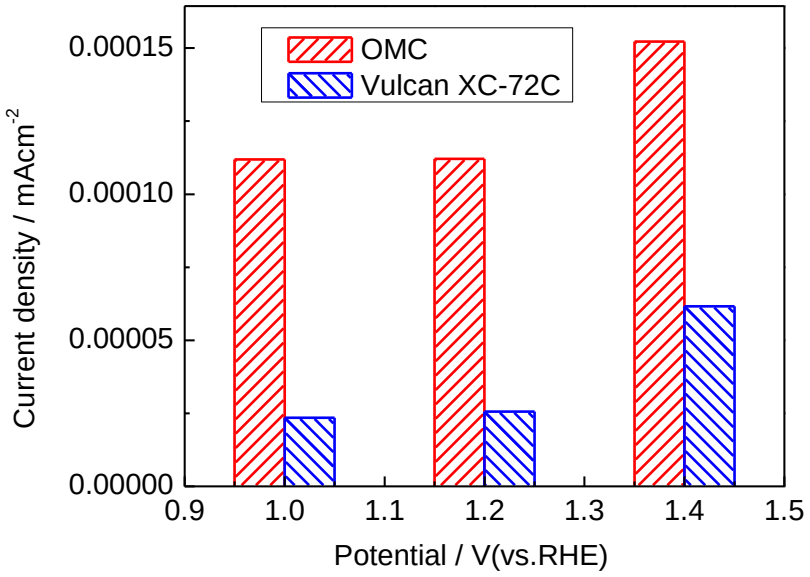

Figure 8. Steady-state anodic current density for the OMC and Vulcan XC-72 supports in 0.1 M $HClO_4$ solution by holding at different potentials for 15 min

However, for the Pt/OMC catalyst, there were still a large portion of Pt particles on the order of 3-8 nm, which should result from the confining effects of mesopores of OMC on Pt particles. This confinement could explain well the long-term durability of Pt/OMC catalyst as revealed by the EASA results in Fig. 6.

During the durability tests, electrocatalytic activity of the Pt/OMC and Pt/C catalysts towards OR reaction was measured using an RDE method. Fig. 9A and 9B show OR LSV curves for the two catalysts. Clearly, these curves were typically divided into three regions: the kinetically controlled (> 0.85 V), the mixed controlled (0.6–0.85 V), and the diffusively controlled (< 0.6 V) regions [12]. The OR activity in the kinetically controlled region is mainly determined by the EASA, crystallinity and surface electronic state of Pt particles, whereas that in the diffusively controlled region is governed by the diffusion of oxygen. In the diffusively controlled region, the OR activities of Pt/OMC catalyst were slightly lower than those of Pt/C, which was believed to be caused by the slow diffusion of oxygen in the OMC pores. In the kinetically controlled region, the OR activities of the Pt/OMC and Pt/C catalysts at 0.85 V are compared in Fig. 9C. Before durability tests, the pristine Pt/OMC catalyst exhibited 33% higher activity towards OR reaction than Pt/C. This higher activity might result from the tailored surface electronic state of Pt particles by the OMC support [30], in addition to the larger EASA as revealed by Fig. 6, because the EASA of Pt/OMC was only 14% higher than that of Pt/C. After durability tests, the OR activities of the two catalysts were reduced as a result of the lowered EASA. However, it was interesting that the OR activity of Pt/OMC was always higher than that of Pt/C after the durability tests, even though the EASA of Pt/OMC was already lower than that of Pt/C.

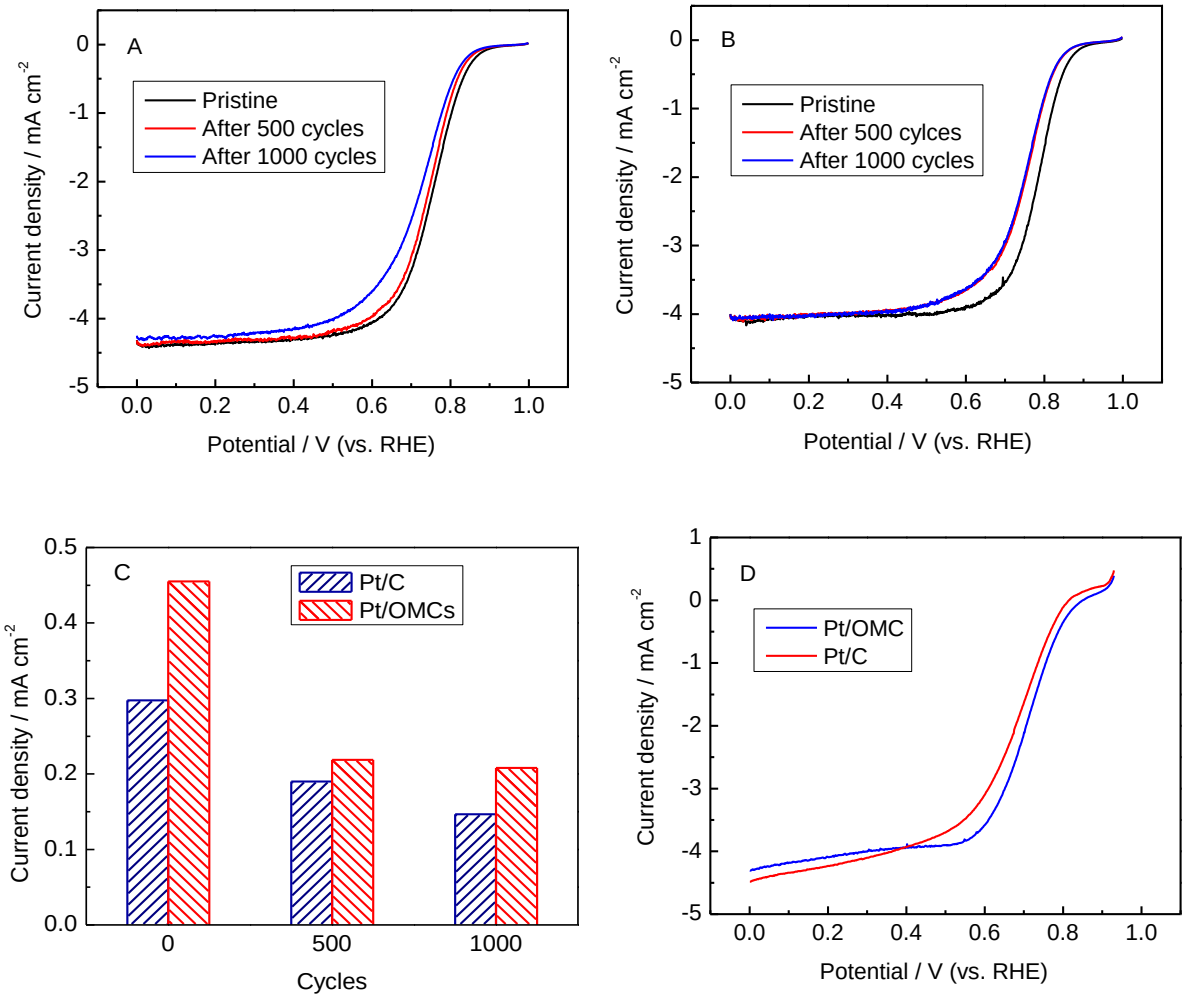

Figure 9. LSV curves of the Pt/C (A) and Pt/OMC (B) catalysts and their OR activities at 0.85 V (C) in 0.1 M $HClO_4$ solution saturated with O_2, and LSV curves of the catalysts after 1000 cycles of durability tests in 0.5 M H_2SO_4 + 10 μM HCOOH solution saturated with O_2 (D) (rotating rate: 900 rpm)

In addition, after 500 cycles of durability tests, the OR activity of Pt/OMC catalyst decreased slightly, whereas that of Pt/C still degraded steadily. This more durable activity for Pt/OMC catalyst could be attributed to its more metallic Pt as demonstrated by XPS results [31] and long-term EASA stability discussed above. To evaluate the catalyst activity in the practical cathode working condition of DFAFC, the response of the ORR in the presence of formic acid on the aged catalysts was obtained in 0.5 M H_2SO_4 + 10 μM HCOOH solution. Fig. 9D gives the OR LSV curves for the aged Pt/C and Pt/OMC catalysts. Compared with the pristine ones, both the catalysts showed a significant increase in OR overpotential in the presence of formic acid due to the competitive reactions of OR and FAO, which results in the formation of a mixed potential. However, even after the durability test, the Pt/OMC catalyst still exhibited higher catalytic activity for OR than Pt/C in the presence of formic acid. Thus, the Pt/OMC catalyst can be used as a more durable formic-acid resistant cathode catalyst for the DFAFC.

Electrocatalytic activities of the Pt/OMC and Pt/C catalysts towards FAO reaction were also quantified by CV curves illustrated in Fig. 10. For both catalysts, on positive scan, the first current peak at ~0.43 V was mainly assigned to the direct FAO (direct path) and the second peak at ~0.88 V corresponded to the FAO via CO as a reaction intermediate (CO path) [32]. With the poisoning species consumed in the positive scan, the current densities attained a higher peak at ~0.44 V in the subsequent negative scan. Before durability tests, all the current peaks for Pt/OMC were slightly higher than those for Pt/C. After 1000 cycles of durability tests, these current peaks were substantially reduced. However, the reduction for Pt/OMC was more severe than that for Pt/C. This activity variation was roughly in agreement with the EASA values during the durability tests, suggesting that Pt/OMC was less active and durable for FAO than for OR reactions. The detailed reason for this difference was still unclear, and might be due to the fact that the tailoring of OMC on Pt particles did not positively contribute to the kinetics of FAO.

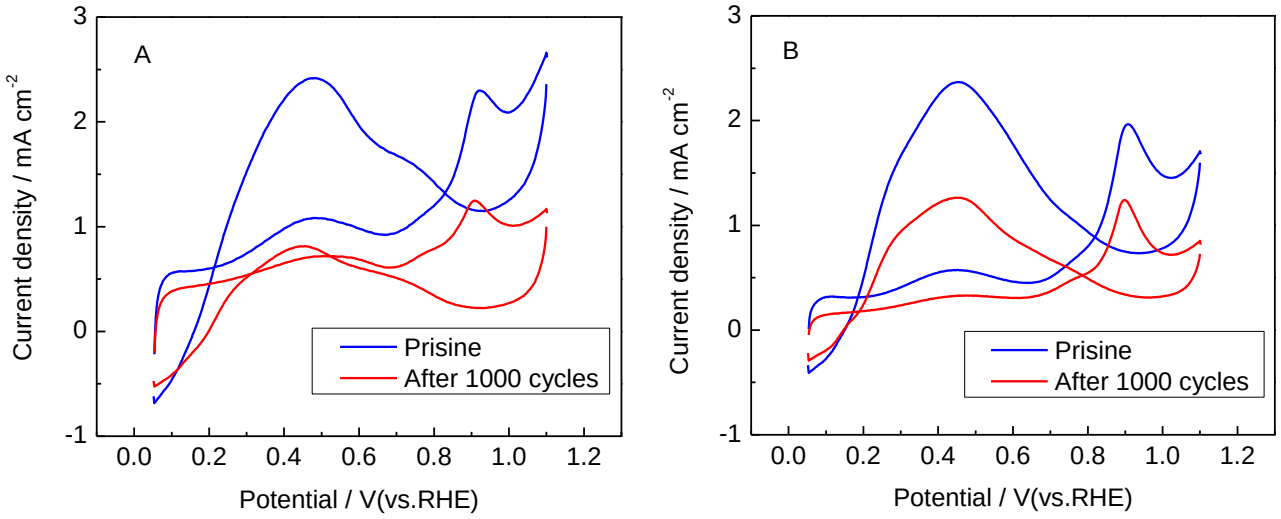

Figure 10. CV curves of the Pt/OMC (A) and Pt/C (B) catalysts after different cycles of durability tests in 0.1 M $HClO_4$ and 0.5 M HCOOH solution at a scan rate of 50 mV s^{-1}

4. CONCLUSIONS

This study prepared OMC supported Pt particles (Pt/OMC) and evaluated their durability as catalysts for DFAFCs. High surface area and ordered mesopores of the OMC support lead to a smaller average size and narrower size distribution of Pt particles. Thus, the Pt/OMC catalyst has higher initial activities towards the reactions of OR and FAO, relative to the conventional Pt/C catalyst. During ageing, due to the confining effects of mesopores of OMC on Pt particles, the Pt/OMC catalyst exhibits better long-term durability than Pt/C, although its short-term durability is relatively lower. More importantly, after ageing, the activity and formic-acid resistance of Pt/OMC catalyst towards OR are still much higher than those of Pt/C, which are attributed to the intrinsic catalytic enhancement from the tailoring by the OMC support. In contrast, the activity of Pt/OMC towards FAO after ageing

is lower than that of Pt/C. Therefore, the Pt/OMC catalyst is promising as a durable and robust cathode catalyst for DFAFCs.

ACKNOWLEDGEMENTS
This work was supported by the National Science Foundation of China under contract No. 20706010 and 20876029, the Harbin Talents Foundation in the Innovation of Science and Technology under contact No. 2008RFQXG059, and the Natural Scientific Research Innovation Foundation in Harbin Institute of Technology.

References

1. W. Qian, D. Wilkinson, J. Shen, H. Wang and J. Zhang, *J. Power Sources*, 154 (2006) 202.
2. S. Ha, B. Adams and R. Masel, *J. Power Sources*, 128 (2004) 119.
3. X. Wang, Y. Tang, Y. Gao and T. Lu, *J. Power Sources*, 175 (2008) 784.
4. J. Wang, G. Yin, Y. Chen, R, Li and X. Sun, *Int. J. Hydrogen Energy*, 34 (2009) 8270.
5. J. Lović, A. Tripković, S. Gojković, K. Popović, D. Tripković, P. Olszewskic and A. Kowal, *J. Electroanal. Chem.*, 581 (2005) 294.
6. S. Uhm, S. Chung and J. Lee, *Electrochem. Commun.*, 9 (2007) 2027.
7. S. Park, Y. Xie and M. Weaver, *Langmuir*, 18 (2002) 5792.
8. X. Wang, W. Li, Z. Chen, M. Waje and Y. Yan, *J. Power Sources*, 158 (2006) 154.
9. M. Sevilla, C. Sanchis, T. Valdes-Solis, E. Morallon and A. Fuertes, *J. Phys. Chem. C*, 111 (2007) 9749.
10. H. Kim, D. You, H. Yoon, S. Joo, C. Pak, H. Chang and I. Song, *J. Power Sources*, 180 (2008) 724.
11. P. Shanahan, L. Xu, C. Liang, M. Waje, S. Dai and Y. Yan, *J. Power Sources*, 185 (2008) 423.
12. S. H. Joo, H. I. Lee, D. J. You, K. Kwon, J. H. Kim, Y. S. Choi, M. Kang, J. M. Kim, C. Pak, H. Chang, D. Seung, *Carbon*, 46 (2008) 2034.
13. E. Ambrosio, C. Francia, M. Manzoli, N. Penazzi and P. Spinelli, *Int. J. Hydrogen Energy*, 33 (2008) 3142.
14. S. H. Joo, S. J. Choi, I. Oh, J. Kwak, Z. Liu, O. Terasaki and R. Ryoo, *Nature*, 412 (2001) 169.
15. S. H. Joo, C. Pak, D. J. You, S. A. Lee, H. I. Lee, J. M. Kim, H. Chang and D. Seung, *Electrochim. Acta*, 52 (2006) 1618.
16. J. Ding, K. Chan, J. Ren and F. Xiao, *Electrochim. Acta*, 50 (2005) 3131.
17. J. Salgado, F. Alcaide, G. Alvarez, L. Calvillo, M. Lazaro and E. Pastor, *J. Power Sources*, 195 (2010) 4022.
18. S. Joo, K. Kwon, D. You, C. Pak, H. Chang and J. Kim, *Electrochim. Acta*, 54 (2009) 5746.
19. R. Rioux, H. Song, J. Hoefelmeyer, P. Yang and G. Somorjai, *J. Phys. Chem. B*, 109 (2005) 2192.
20. M. Tsuji, M. Kubokawa, R. Yano, N. Miyamae, T. Tsuji, M. Jun, S. Hong, S. Lim, S.-H. Yoon and I. Mochida, *Langmuir*, 23 (2007) 387.
21. T. Koranyi, Z. Vit, D. Poduval, R. Ryoo, H. Kim and E. Hensen, *J. Catalysis*, 253 (2008) 119.
22. Y. Wang, F. Su, C. Wood, J. Lee and X. Zhao, *Ind. Eng. Chem. Res.*, 47 (2008) 2294.
23. J. Kim, C. Shin and R. Ryoo, Catal. Today, 38 (1997) 221.
24. A. Pozio, M. De Francesco, A. Cemmi, F. Cardellini and L. Giorgi, *J. Power Sources*, 105 (2002) 13.
25. S. Vengatesan, H.-J. Kim, S.-K. Kim, I.-H. Oh, S.-Y. Lee, E. Cho, H. Y. Ha and T.-H. Lim, Electrochim. Acta, 54 (2008) 856.
26. J. Moulder, W. Stickle, P. Sobol and K. Bomben, *Handbook of X-Ray Photoelectron Spectroscopy*, Perkin-Elmer Physical Electronics Division, Eden Prairie MN (1992).

27. U. Zielke, K. Huttinger and W. Hoffman, *Carbon*, 34 (1996) 983.
28. X. Yu and S. Ye, *J. Power Sources*, 172 (2007) 145.
29. K. Kinoshita, D. Ferrier and P. Stonehart, *Electrochim. Acta*, 23 (1978) 45.
30. J. Salgado, J. Quintana, L. Calvillo, M. Lázaro, P. Cabot, I. Esparbé and E. Pastor, *Phys. Chem. Chem. Phys.*, 10 (2008) 6796.
31. T. Nagai, H. Murata and Y. Morimoto, *Analysis of the Relation between Oxidation State and ORR Activity of Pt by Linear Sweep Voltammetry*, 218th ECS Meeting, Las Vegas NV (2010).
32. O. Wolter, J. Willsau and J. Heitbaum, *J. Electrochem. Soc.*, 132 (1985) 1635.